Astron. Astrophys. 241, 589–594 (1991)

ASTRONOMY AND ASTROPHYSICS

An optical and infrared study of the reflection nebulae GGD 30 and GGD 31

A.I. Gómez de Castro and C. Eiroa

Observatorio Astronómico de Madrid – IGN, c/Alfonso XII, 3, E-28014 Madrid, Spain

Received December 29, 1989; accepted July 15, 1990

Abstract. CCD images and near-IR observations of the nebular objects GGD 30 and GGD 31 are presented. The data have been used to study the morphology and physical nature of the nebulosities. GGD 30 is a reflection nebula illuminated by a low mass PMS star of estimated luminosity $\approx 2.3\,L_{\odot}$. The CCD images reveal that the illuminating star is likely to be double with a separation between components of 4″, corresponding to a projected linear separation of 2000 AU. A stream arises from one of the stellar components; our data do not show, however, evidence of shock-excited material. GGD 31 is a reflection nebula showing a rather complex morphology. It has a dark cavity within the nebulosity and there are two nebular streams arising from the illuminating star and surrounding the cavity. The estimated luminosity of the star is $\approx 10\,L_{\odot}$.

In addition, the region around GGD 30 has been surveyed in the near-IR and also searched for IRAS point sources. A further PMS object is present in the GGD 30 region. Finally, a peculiar near-IR object has been detected. The object seems to be a late type oxygen-rich star with very extreme colours, $H-K=4.47$, $K-L'=4.49$, and $L'-M'=1.19$ mag.

Key words: infrared radiation – interstellar medium: reflection nebulae: GGD 30, GGD 31 – stars: pre-main-sequence

1. Introduction

GGD objects are small red nebulosities located in the galactic plane initially suspected to be Herbig-Haro objects (Gyulbudaghian et al. 1978). Optical observations have shown that many of them are reflection nebulae (e.g. Hartigan & Lada 1985; hereafter HL). Rodriguez et al. (1980) reported the detection of CO and NH_3 molecular emission, radio continuum sources and H_2O masers associated with the GGD objects. In some cases, cold molecular outflows have been observed (see Lada 1985). In addition, infrared observations have shown that the GGD nebulosities are normally related to young stars of low to intermediate luminosity (e.g. Reipurth & Wamsteker 1983; Carballo et al. 1988). In summary, GGD objects seem to be good tracers of star forming regions.

In this work we present an optical and infrared study of GGD 30 and GGD 31, as well as of the region around GGD 30. They are the only two northern GGD objects for which IR observations do not exist yet. GGD 30 and GGD 31 are located in different regions of the sky. GGD 30 is an arc-shaped nebulosity located close to the compact H II region G34.3+0.1 (Habing & Israel, 1979). GGD 31 is located in the line of sight of Cygnus X. Optical CCD images of GGD 31 have been reported previously by HL. Molecular emission in the GGD 31 region is complex with multiple velocity components (Blitz 1980), what makes very difficult to sort out whether there is a molecular outflow (Edwards Snell 1983). Rodriguez et al. (1980) give a kinematical distance of 500 pc for both objects on the basis of CO velocities. This is the distance we will assume throughout this work.

This work is structured as follows: Observations are summarized in Sect. 2. GGD 30 and the region around the nebulosity are analyzed in Sect. 3 where it is also reported the discovery of the peculiar infrared source GGD 30/IRS 1. Finally, Sect. 4 is devoted to the study of GGD 31 and the infrared source associated with it.

2. Observations

2.1. Optical

CCD images of GGD 30 and GGD 31 were carried out in August 1985 at the prime focus of the 3.5 m telescope on Calar Alto Observatory; additional images of GGD 30 were obtained in July 1988. The 1985 images were taken using a 576 × 385 pixel GEC CCD, pixel size 22 μm. The scale on the focal plane is 0.″288/pixel and the field of view 166″ × 110″. Images of GGD 31 were obtained with the broad-band filters: $I(\lambda_0 \cong 0.9\,\mu m)$, $R(\lambda_0 \cong 0.7\,\mu m)$, and the narrow band filters Hα ($\lambda_0 = 6657$ Å, FWHM = 100 Å) and [S II] ($\lambda_0 = 6730$ Å, FWHM = 95 Å). Only an I image of GGD 30 was obtained in 1985. The seeing was $\approx 1''$–$2''$. Very short I frames of the stars SAO 069973 and SAO 123980 were carried out immediately before each I object image; these stars have been used as offset stars. Coordinates of point sources associated with GGD 30 and GGD 31 are given in Table 1. GGD 30 was observed again in 1988. This time a CCD RCA of 1024 × 640 pixels was used, pixel size 15 μm. The scale on the focal plane is 0.″258 pixel and the field of view 263″ × 175″. The filters used were I, R and Hα. Seeing conditions were $\approx 1''$. No changes were observed in the GGD 30 I image when compared with the 1985 observations. Flat field correction and dark subtraction of each object frame have been made following standard procedures. Figure 1 shows the RG 830 CCD image of GGD 30 taken in 1988, whereas isocontours plots of the GGD 30 and GGD 31 nebulosities are shown in Figs. 3 and 5 respectively.

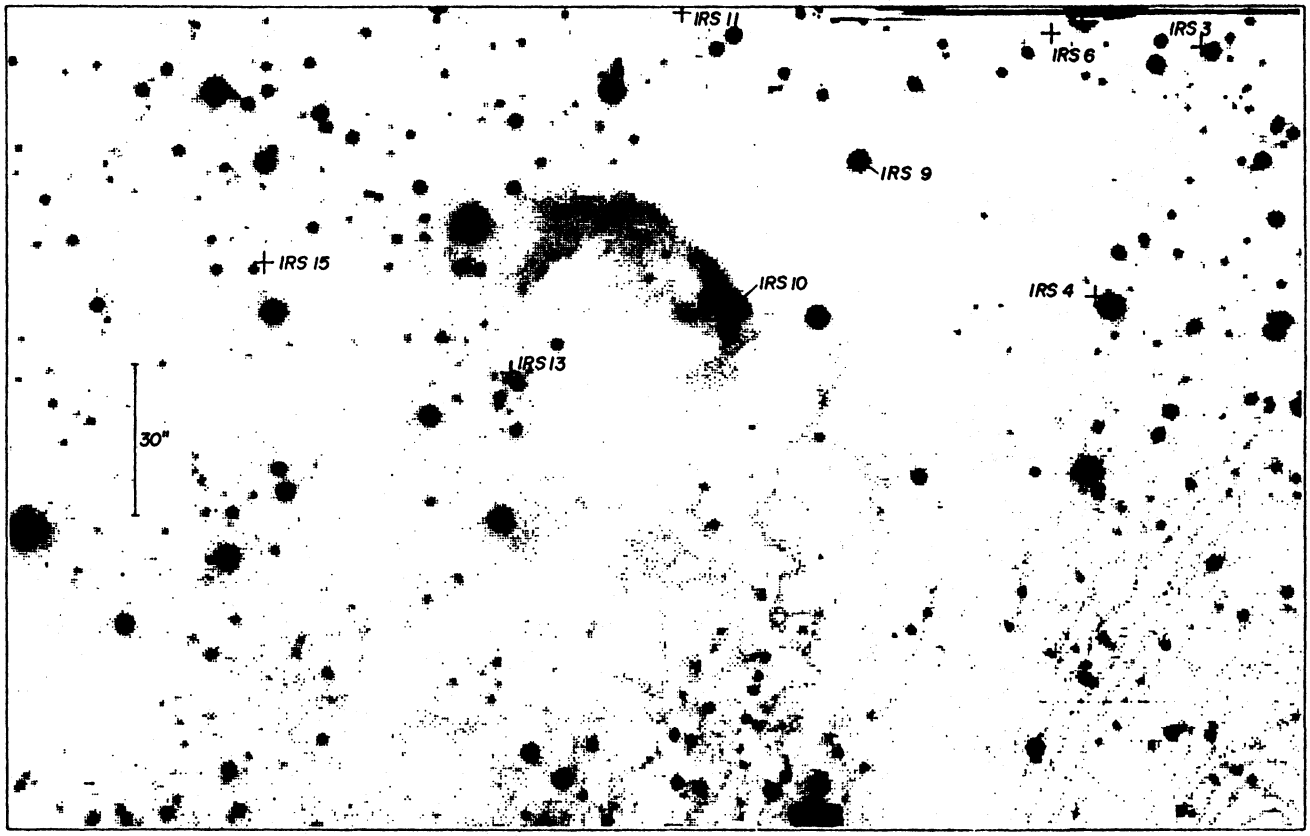

Fig. 1. I image of the GGD 30 field. The contrast is arbitrary. The position of the near-infrared sources detected within the field is indicated. GGD 30 is the nebulosity in the center of the frame. North is at the top and east to the left

Table 1. Point-like sources and condensations in GGD 30 and GGD 31

Source	α(1950)	δ(1950)	Other identification
GGD 30/*I*1	$18^h49^m07^s.2$	00°25′23″	
/*I*2	07.3	25 19	
/*I*3	10.8	25 40	
GGD 31/*I*1	$20^h23^m06^s.9$	39°01′19″	HL 29
/*I*2	07.3	01 35	HL 30
/*C*1	08.1	01 31	
/*C*2	08.3	01 20	HL 31

2.2. *Infrared*

K (2.2 μm) raster scans of the GGD 30 field were carried out in September 1986 at the Calar Alto 1.23 m telescope. A beam size and a chopper throw of 20″ and 30″ respectively were chosen. Three overlapping areas around GGD 30 were scanned: [$18^h48^m57^s.4$, 00°24′23″: $18^h49^m05^s.4$, 00°26′23″], [$18^h49^m04^s.1$, 00°24′23″: $18^h49^m12^s.1$, 00°26′23″], and [$18^h49^m00^s.1$, 00°25′13″: $18^h49^m16^s.1$, 00°27′23″]. The chopper throw was taken in δ direction in the two first maps and in α in the last one. The limiting magnitude was ≈11 mag. 16 sources were detected; one of them, GGD 30/IRS 10, is associated with the GGD 30 nebulosity. The IR sources located within the field of Fig. 1 are indicated in that figure. In addition, *JHKL′M′* photometry of the GGD 30 near-IR sources was carried out at the 3.8 m UKIRT telescope at Mauna Kea Observatory during the nights of June 29th and 30th, 1987. This time an aperture of 7″.8 and a chopper throw of 20″ in δ-direction were selected. Coordinates and magnitudes of the objects as measured at UKIRT are given in Table 2.

Finally, near-IR photometry of GGD 31 was carried out at UKIRT. Position and magnitudes of this object are also given in Table 2.

2.3. *IRAS sources*

We have carried out a search for IRAS sources within an area of 25′ × 25′ around GGD 30, thus including the entire region rastered at 2.2 μm. 18 IRAS point sources have been found; one of them, IRAS 18490+0026, is associated with the near-IR source GGD 30/IRS 3. Table 3 reports positions and flux densities of the sources as given in the IRAS Catalogs and Atlases (Beichman et al. 1988). According to the conventions used in the Catalogs, a colon after the flux densities in Table 3 denotes an uncertain quality measurement, and an "*L*" denotes an upper limit.

Finally, GGD 31 coincides with the source IRAS 20231+3901, the coordinates and fluxes of which are also given in Table 3.

Table 2. Positions and *JHKL'* photometry in magnitudes of GGD 30 and GGD 31

Source	α(1950)	δ(1950)	*J*	*H*	*K*	*L'*
GGD 30						
IRS 1 [a]	$18^h48^m57^s.3$	0°24′48″		14.69±0.09	10.02±0.01	5.53±0.01
IRS 2	48 59.4	24 25	15.00±0.02	13.65±0.02	13.19±0.02	
IRS 3	49 00.6	26 16	13.32±0.01	10.04±0.01	7.51±0.01	4.75±0.01
IRS 4	49 02.3	25 21	11.32±0.01	9.40±0.01	8.54±0.01	8.12±0.01
IRS 5	49 02.7	24 51	11.19±0.02	9.12±0.03	8.30±0.01	7.69±0.02
IRS 6	49 02.8	26 17	11.91±0.01	10.53±0.01	9.88±0.01	9.44±0.06
IRS 7	49 04.2	27 11	8.94±0.01	7.69±0.01	7.24±0.01	6.92±0.01
IRS 8	49 05.3	27 51	9.84±0.01	7.77±0.01	6.70±0.01	5.74±0.01
IRS 9	49 05.6	25 52	12.21±0.01	10.32±0.01	9.55±0.01	9.02±0.04
IRS 10	49 07.4	25 23	12.90±0.02	11.32±0.02	9.78±0.01	6.68±0.01
IRS 11	49 08.1	26 14	12.88±0.01	11.56±0.01	11.08±0.01	10.98±0.07
IRS 12	49 09.9	26 36	12.20±0.01	10.00±0.01	8.94±0.01	8.24±0.01
IRS 13	49 10.3	25 10	11.74±0.01	8.93±0.01	7.60±0.01	6.69±0.01
IRS 14	49 11.0	26 50	11.65±0.01	10.27±0.01	9.72±0.02	9.26±0.06
IRS 15	49 13.7	25 22	9.85±0.01	7.28±0.01	6.01±0.01	5.02±0.01
IRS 16	49 14.9	27 30	13.27±0.01	10.94±0.01	9.91±0.01	9.14±0.02
GGD 31						
IRS [b]	$20^h23^m07^s.0$	39°01′19″	12.34±0.02	10.20±0.01	8.85±0.02	7.37±0.02

[a] $M' = 4.34 \pm 0.02$ for GGD 30/IRS 1
[b] $M' = 5.16 \pm 0.02$ for GGD 31/IRS

Table 3. IRAS sources in the GGD 30 region and the source associated with GGD 31

Source	α(1950) (s)	δ(1950) (″)	*F*(12 μm) (Jy)	*F*(25 μm) (Jy)	*F*(60 μm) (Jy)	*F*(100 μm) (Jy)
18490+0026 [a]	0.9	13	10.12L	24.53	69.65:	294.81L
18490+0022	2.6	23	3.55L	1.62	28.37:	382.38L
18492+0015	15.5	50	3.86L	7.53	116.05:	1146.10L
18493+0025	21.4	31	3.82L	5.33L	16.60	266.63L
18493+0030	21.7	16	1.30:	10.01L	47.32:	266.63
18494+0010	24.0	31	13.87:	88.34	826.12	2178.94L
18495+0026	35.4	32	3.17L	3.59	25.79L	2064.42
18495+0014	35.6	48	1.43:	6.44	85.45:	2178.94L
18496+0004	36.2	59	3.25:	24.11	591.42	2178.94
18496+0030	36.3	53	13.28:	9.97	18.81L	269.44L
18497+0022	46.4	6	13.43L	31.17L	546.02	2064.42
18498+0028	53.1	28	4.11	11.31	72.94:	175.61L
18499+0026	57.5	3	3.43L	7.12	62.47	2064.42L
18499+0017	58.0	7	1.35	0.79L	12.88L	2064.43L
18500+0010	5.6	29	2.37	1.27	7.53:	256.62L
18501+0013	6.2	4	4.22	8.70	12.56L	260.16L
18502+0008	15.9	4	3.58	3.02:	11.65L	253.30L
18504+0025	26.9	5	2.55	5.87	98.07:	304.93
20231+3901 [b]	7.0	20	0.67	1.18	28.48L	221.30L

[a] IRAS counterpart of GGD 30/IRS 3
[b] IRAS counterpart of GGS 31/IRS

3. GGD 30

3.1. The two-colour diagram of the near-IR sources

Figure 2 shows the near-IR sources in the two-colour ($J-H, H-K$) diagram. The straight line indicates the reddening law of Rieke & Lebofsky (1985). The curved lines represent the intrinsic colours of normal main-sequence, giants and supergiant stars, spectral types A0 to M5 (Koornneef 1983). Two objects, IRS 3 and IRS 10, show a remarkable infrared excess indicating their PMS nature (e.g. Rydgren & Cohen 1985). IRS 3 is the star associated with the IRAS source 18490+0026, and IRS 10 is associated with the GGD 30 nebulosity. The rest of IR-sources are located along the reddening line and they probably are background stars.

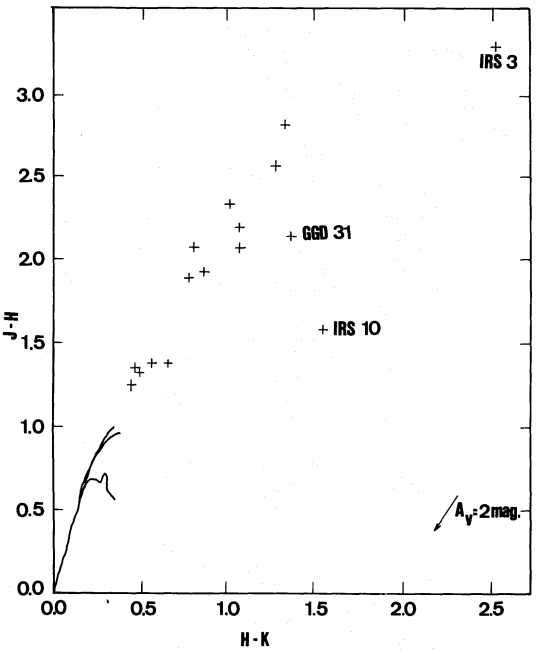

Fig. 2. $J-H, H-K$ diagram of the infrared sources found in the GGD 30 field. The arrow at the bottom indicates the RL reddening line. Curved lines indicate the intrinsic colours for luminosity classes I, III, and V. The position of the PMS stars GGD 30/IRS 3, 10 and GGD 31/IRS is shown

3.2. PMS objects in the GGD 30 region

3.2.1. The nebulosity

GGD 30 is approximately oriented in the east-west direction, with $\approx 50''$ in size, Figs. 1 and 3. Morphologically, it is formed by an arrow-shaped structure at the west of the nebulosity where two point-like sources, $I1$ and $I2$, are observed, and a large diffuse component towards the east. Both nebular structures are separated by a dark region.

$I1$ coincides with the near-IR source IRS 10. The second point-like object, $I2$, is detected $4''$ ($\cong 2000$ AU) south of $I1$; we cannot exclude that $I2$ also contributes to the observed near-IR flux from IRS 10. Several condensations are seen close to both stars; in particular, there is a sharply delineated, well collimated stream which departs from $I1$ towards the north-east in the direction of the diffuse component of GGD 30. There is no clear indication of shock-excited material in the CCD images (see e.g. HL) and, consequently, GGD 30 is most likely a reflection nebula.

The energy distribution of IRS 10 is very red. We can estimate its total luminosity integrating the observed fluxes and assuming that for wavelengths longer than 3.8 μm the energy distribution is given by a blackbody, the maximum flux of which is the flux detected at 3.8 μm. The estimated value is $\approx 2.3\, L_\odot$, which indicates that the star illuminating GGD 30 is a low mass PMS object, similar to most of the stars illuminating the GGD objects.

3.2.2. GGD 30/IRS 3

The near-IR colours of IRS 3 show an infrared excess suggesting its PMS nature. The object is located on the NW of GGD 30 and it seems to have an I counterpart in the CCD images, Fig. 1. IRS 3 is also associated with the IRAS source 18490+0026. The near-IR energy distribution can be fitted with a black body of approximately 800 K, whereas the IRAS fluxes give $T(25/60) \approx 90$ K. The total luminosity of GGD 30/IRS 3 is $< 100\, L_\odot$, assuming that it is associated with the GGD 30 molecular cloud.

3.3. GGD 30/IRS 1

IRS 1 is the most intriguing near-IR source found in the GGD 30 region. The source does not have an optical counterpart in the CCD images and it is in a relatively clear region. IRS 1 has very peculiar infrared colours: $H-K=4.67$, $K-L'=4.49$ and $L'-M'=1.19$, Table 2. For comparison the colours of NML Cyg and IRC +10216, two of the reddest sources in the Galaxy, are $H-K=4.47$, $K-L=2.36$ and $L-M=1.55$ and $H-K=3.00$,

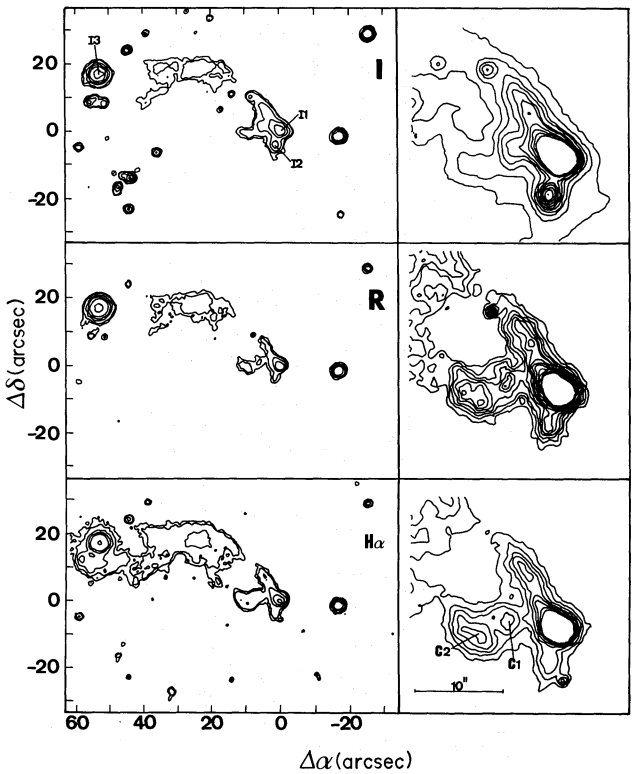

Fig. 3. Isocontour plot of GGD 30. The whole nebulosity is shown in the left panels, whereas the right panels are more detailed plots of the arrow-shaped structure. Top: I filter, middle: R filter, bottom: Hα filter. Isocontours are arbitrary and chosen to show some morphological features

K − L = 3.46 and $L-M=1.5$ respectively, whereas the colours of the highly reddened source observed toward the galactic center, IRS 11, are $H-K=2.18$, K − L = 1.6 and $L-M=1.0$ (Becklin et al. 1978).

We took a 2–4 μm CVF spectrum (2% spectral resolution) of IRS 1 using UKIRT at Mauna Kea Observatory. The infrared spectrum and the broad band photometry are represented in Fig. 4. The spectrum shows the absorption bands of CO and H_2O at 2.3 and 2.7 μm respectively, characteristics of cool oxigen giants (Merrill & Stein 1976). An estimate of the spectral type can be made by means of the [2.35]–[2.2] index (Kenyon & Gallagher 1983). The observed value indicates a M6 III spectral type, although it may be cooler as the IRS 1 index is just at the limits of the correlation of Kenyon and Gallagher. If we assume that IRS 1 is an M6 III star, the optical extinction would be 68 mag (estimate done using the observed $H-K$ colour and the intrinsic value for M6 III stars given by Koornneef (1983)), which is extremely high. Even if we consider an effective temperature of 2000 K (i.e. M9–M10 spectral type) the estimated extinction would also be considerable, $A_v = 48$ mag (estimate done by comparing the IRS 1 energy distribution and that of a 2000 K black body, and assuming that the 2.25 and 3.8 μm observed fluxes are free of absorption (Merrill & Stein 1976)). The high extinction is unlikely to be due to an interstellar origin; for instance, the interstellar extinction towards the galactic center accounts for $A_v = 30$ mag (Becklin & Neugebauer 1968). Thus, the near-IR data suggest that IRS 1 is a very late oxygen-rich M star surrounded by an extremely thick circumstellar dust envelope. On the other hand, there is no IRAS counterpart to IRS 1, and the energy distribution peaks at a wavelength close to 5 μm. This situation is surprising given the notorious dust envelope suggested by the near-IR data and reveals again the singularity of the infrared source GGD 30/IRS 1.

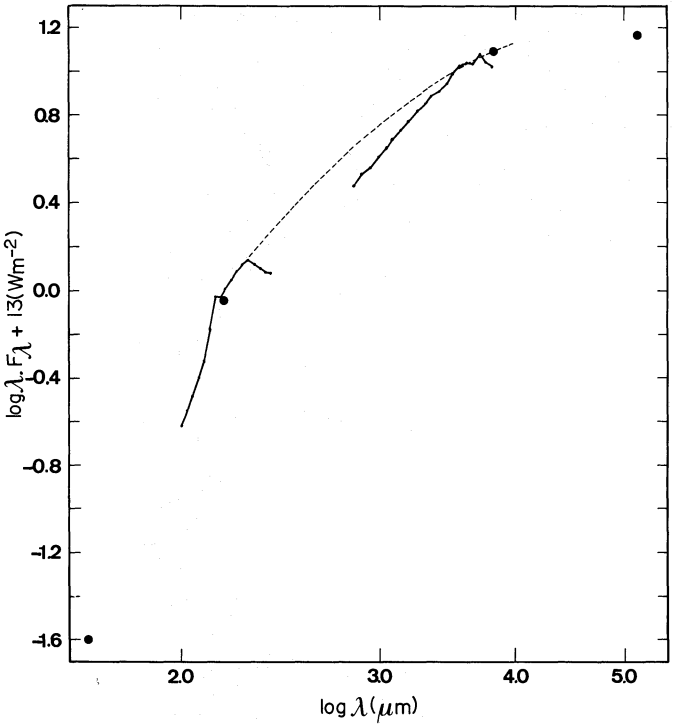

Fig. 4. The energy distribution of GGD 30/IRS 1. Broad band photometry and the CVF spectrum are indicated by black dots and a continuum line respectively. The dashed line represents the assumed continuum level

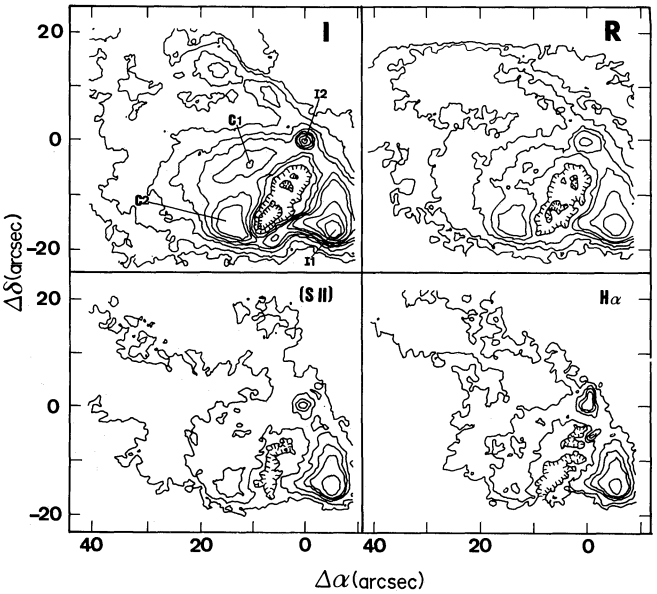

Fig. 5. Isocontour plot of GGD 31. *I*: top left, *R*: top right, [S II]: bottom left, Hα: bottom right. Isocontours drawn in the three last images are 3, 6, 12, 24, and 48σ, whereas in the *I* image the levels 36, 96, 192, and 384σ are also included. Point sources and some condensations are identified in the *I* frame. The 3σ and 6σ levels surrounding the dark cavity are indicated with small traces perpendicular to the contours. North is at the top and East to the left

4. GGD 31

GGD 31 is a reflection nebula of around 45″ × 45″ in size and showing a rather complex morphology, Fig. 5. Two point-like sources, *I*1 (HL 29) and *I*2 (HL 30), together with several condensations are observed in the nebulosity. Coordinates are given in Table 1. The condensation C2 corresponds to the object 31 of HL. Estimated *I* magnitudes of the stars *I*1 and *I*2 are 15.3 and 17.3 mag respectively, in satisfactory agreement with the HL's results, the small differences being probably due to the different effective wavelengths and to the contamination produced by the nebulosity.

A near-IR and an IRAS source are associated with *I*1, Tables 1–3. The colours $J-H$ and $H-K$ show an IR excess indicating the PMS nature of the star, Fig. 2. The near-infrared density fluxes can be fitted with a black body of ≈1300 K; in addition, the IRAS temperature $T(12/25)$ is $T \approx 230$ K. The total luminosity of the source is $L \approx 10\,L_\odot$.

The nebula has a dark cavity (flux minimum) of 13″ × 6″ in size apparently splitted in two components at very low signal levels. Two nebular streams arising from *I*1 surround the cavity. The southern stream extends to the east and presents a large isocontour gradient; the condensation C2 is observed at the end of this stream. The second stream is directed towards the north in the direction of the star *I*2, and extends to the northeast forming a nebular arm far away from the main body of GGD 31. We can qualitatively study the reddening within the nebula by means of the $[R-I]$ colour map, Fig. 6. There is a bar arising from *I*1, extending towards the east in the direction of the cavity and approximately coinciding with the southern stream. The colour in the body of the bar is very high when compared with the mean colour of the nebulosity (up to ≈1.0 mag over the nebular values). The colour gradient is very pronounced between the southern part of the cavity and the edge of the nebulosity, which is progressively

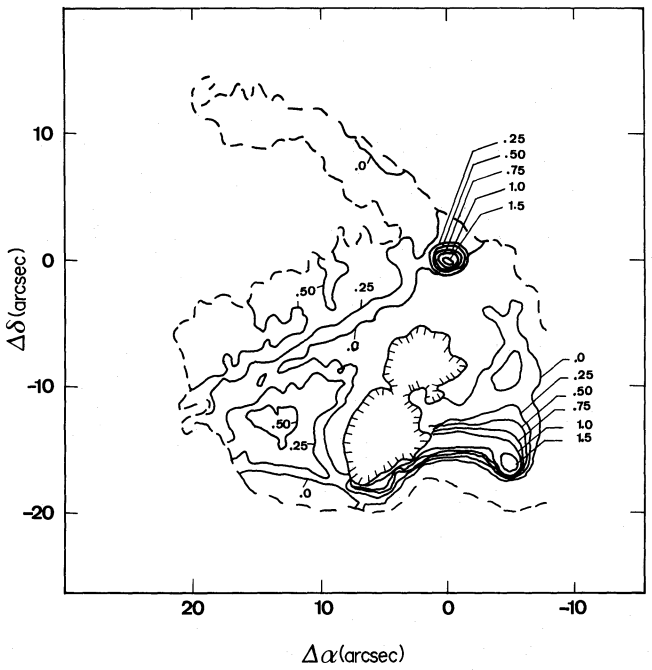

Fig. 6. [$R-I$] map of GGD 31. Isocontours showing different reddening are plotted. The $R-I$ colours are in instrumental magnitudes without zero point correction. The lower level has been arbitarily considered as the one with relative reddening equal to 0.0 mag. North is at the top and east to the left

redder when approaching the cavity. On the other hand, a smooth bluing is observed to the north of $I1$ in the direction of the second nebular stream.

It does not seem to be a simple task to explain the morphology and colours of GGD 31, which are probably related to the anisotropic mass loss observed in the early phases of stellar evolution. A crude and simple explanation would be that the cavity (flux minimum in the images) is a region of enhanced dust density acting as a wall. In this case, the nebular gas would surround this wall leading to the formation of the streams by the stellar wind of the PMS source GGD 31/$I1$. In addition, far away from the star and the stream, i.e. the eastern part of GGD 31 and the nebular arm, the behaviour of the colours are typical of reflection nebulae.

Acknowledgements. We are very grateful to the Calar Alto and UKIRT staffs, in particular to. M. Casali, for their help during the observations, as well as ESA for the use of their computer facilities in VILSPA. We also thank R. Carballo for her useful comments. The Calar Alto Observatory is operated jointly by the Max-Planck-Institut für Astronomie (Heidelberg) and the Spanish Comisión Nacional de Astronomía. UKIRT (United Kingdom Infrared Telescope) is operated by the Royal Observatory of Edinburgh on behalf of the U.K. Science and Engineering Research Council. A.I.G. is supported by a fellowship of the Spanish Ministerio de Educación y Ciencia. This work has been supported in part by grant DGICYT PB87-0167

References

Becklin E.E., Neugebauer G., 1968, ApJ 151, 145
Becklin E.E., Matthews K., Neugebauer G., Willner S.P., 1978, ApJ 219, 121
Beichman C.A., Neugebauer G., Habing H.J., Clegg P.E., Chester T.J., 1988, Infrared Astronomical Satellite (IRAS). Catalogs and Atlases, NASA RP-1190
Blitz L., 1980, Giant Molecular Clouds in the Galaxy, eds. P.M. Solomon, M.C. Edmunds, Pergamon Press, Oxford, New York
Carballo R., Eiroa C., Mampaso A., 1988, MNRAS 232, 497
Edwards S., Snell R.L., 1983, ApJ 270, 605
Gyulbudaghian A.L., Glushkov Yu.I., Denisyuk E.K., 1978, ApJ 224, L137 (GGD)
Habing H.J., Israel F.P., 1979, ARA & A 17, 345
Hartigan P., Lada C.J., 1985, ApJS 59, 383 (HL)
Kenyon S.J., Gallagher J.S., 1983, AJ 88, 666
Koornneef J., 1983, A & A 128, 84
Lada C.J., 1985, ARA & A 23, 267
Merrill K.M., Stein W.A., 1976, PASP 88, 294
Reipurth B., Wamsteker W., 1983, A & A 119, 14
Rieke G.H., Lebofsky M.J., 1985, ApJ 288, 618
Rodriguez L.F., Moran J.M., Ho P.T.P., Gottlieb E.W., 1980, ApJ 235, 845
Rydgren A.C., Cohen M., 1985, Protostars and Planets II, eds. D.C. Black, M.S. Matthews, University of Arizona Press, Tucson, p. 371